

Towards spin turbulence of light: Spontaneous disorder and chaos in cavity-polariton systems

S. S. Gavrilov

Institute of Solid State Physics, RAS, Chernogolovka, Russia

(Dated: November 2, 2016)

Recent advances in nanophotonics have brought about coherent light sources with chaotic circular polarization; a low-dimensional chaotic evolution of optical spin was evidenced in laser diodes. Here we propose a mechanism that gives rise to light with a spatiotemporal spin chaos resembling turbulent states in hydrodynamics. The spin-chaotic radiation is emitted by exciton polaritons under resonant optical pumping in arbitrarily sized planar microcavities, including, as a limiting case, pointlike systems with only three degrees of freedom. The underlying mechanism originates in the interplay between spin symmetry breakdown and scattering into pairs of Bogolyubov excitations. As a practical matter, it opens up the way for spin modulation of light on the scale of picoseconds and micrometers.

PACS numbers: 71.36.+c, 42.65.Sf, 42.50.Pq

I. INTRODUCTION

Deterministic spin chaos has been recently detected in laser diodes [1], promising impressive applications in the field of information encoding and transmission, fast random number generation, cryptography, etc. [2] Today, however, only a low-dimensional chaotic evolution of optical spin is achieved; also known are externally shaped [3] as well as spontaneous [4] spin patterns. In this work we address the problem of making spin of light reveal a *spatiotemporal* chaos ([5]), similar to turbulent fluids with high-dimensional chaotic attractors. We have found that light with such properties can be emitted by the system of cavity polaritons, half-light half-matter excitations in microcavities.

Cavity polaritons are composite bosons originating due to the strong coupling of excitons (electron-hole pairs in semiconductors) and cavity photons [6–8]. They are known to form macroscopically coherent states in two ways. The first is Bose-Einstein condensation, occurring as a phase transition under nonresonant optical pumping [9, 10]. The other way is direct resonant and coherent driving that immediately governs both density and phase of a *highly nonequilibrium* polariton condensate [11, 12]. Since excitons are strongly coupled to externally driven cavity photons, they share a unified quantum state rather than just constitute a nonlinear medium for propagating light.

It has long been accepted that chaotic polariton states are feasible only in inhomogeneous systems and appear due to the Josephson effect. Josephson oscillations in superconducting junctions occur between coupled coherent modes whose phase difference varies with time [13]; analogous phenomena were observed in Bose-Einstein condensates of cold atoms [14] and cavity polaritons [15, 16]. The Josephson effect is, however, hardly possible in spatially homogeneous condensates formed under resonant plane-wave driving. Polaritons have very small lifetime, hence a constant harmonic pump force makes them oscillate at exactly the same frequency, similar to a usual damped pendulum. Since the spin-up and spin-down components have constant phase difference, their interchange—often referred to as intrinsic Josephson effect [17]—is also prevented. Such a system can only be *multistable* [18, 19] because of the polariton-polariton interaction.

Switches between distinct steady-state branches reveal themselves as sharp jumps in the cavity field [20–26]. Thus, the very short lifetime of polaritons ($\tau \sim 10^{-11}$ s in GaAs-based microcavities) makes them interesting in view of fast optical switches, but on the other hand, it usually forbids long-lived transient or unsteady states in a spatially homogeneous and truly constant environment.

Here we report a mechanism lifting the above limitation. We consider an internally homogeneous spinor polariton system pumped at normal incidence and show that its well-known multistable behavior can be turned into deterministic chaos. This happens when a spontaneously broken spin symmetry of the condensate ([27, 28]) starts being restored through Bogolyubov excitations, which essentially relies on the non-Hermitian nature of polaritons and would be impossible in ordinary Bose-Einstein condensates close to thermal equilibrium.

Previously, both oscillatory [29] and chaotic [30, 31] polariton states were theoretically considered in a double-well geometry resembling a Josephson junction. The Josephson oscillations of polaritons were observed under non-resonant excitation [15, 16]. It is also reported that the combination of spatially separated resonant and nonresonant pump sources is capable of producing a chaotic spin state at a certain location [28, 32]. These mechanisms are limited to particular excitation geometries and deliver only low-dimensional chaos. In its turn, our mechanism ensures a spatiotemporal spin chaos in arbitrarily sized polariton systems, from pointlike micropillars to uniform planar cavities.

The following Section II describes the model and the instabilities leading to the chaotic behavior which is then analyzed in the cases of pointlike systems (Sec. III) and large cavities (Sec. IV).

II. SPIN SYMMETRY BREAKDOWN

Coherent polariton states are described by the spinor Gross-Pitaevskii equation [8],

$$i\hbar \frac{\partial \psi_{\pm}}{\partial t} = (\hat{E} - i\gamma + V\psi_{\pm}^* \psi_{\pm}) \psi_{\pm} + \frac{g}{2} \psi_{\mp} + f_{\pm} e^{-i\frac{E_p}{\hbar} t}. \quad (1)$$

A pair of macroscopic wavefunctions ψ_{\pm} depend on time and spatial coordinates in a two-dimensional active cavity layer. ψ_{+} and ψ_{-} are the spin-up and spin-down components connected directly with the right (σ^{+}) and left (σ^{-}) circular polarizations of the output light. V is the polariton-polariton interaction constant. Polaritons with parallel spins repel each other ($V > 0$) [33–36], which results in a blue shift ($\sim V|\psi^2|$) of their resonance energy. Choosing $V = 1$ determines the units of ψ and f . Operator $\hat{E} = \hat{E}(-i\hbar\nabla)$ implies the dispersion law common for both spin components (see Appendix A); γ is the decay rate. The eigenstates at $\psi_{\pm} \rightarrow 0$ are polarized linearly in the x and y directions so long as $\begin{pmatrix} \psi_x \\ \psi_y \end{pmatrix} = \frac{1}{\sqrt{2}} \begin{pmatrix} 1 & 1 \\ i & -i \end{pmatrix} \begin{pmatrix} \psi_{+} \\ \psi_{-} \end{pmatrix}$ by definition, and $g \equiv E_x - E_y$ is the splitting between them. The incident light wave (“pump”) has spinor amplitude f_{\pm} , frequency E_p/\hbar , and a zero in-plane momentum ($k = 0$), so that it falls perpendicular to the cavity. Let us finally assume $f_{+} = f_{-} = f$; then the pump is x -polarized and the equations for ψ_{+} and ψ_{-} become exactly the same. The plane-wave solutions with $k = 0$ have the form $\psi(t) \propto e^{-i(E_p/\hbar)t}$ for both spin components. Such solutions always exist in a spatially homogeneous system, however, they can be unstable.

The exact spin symmetry ($\psi_{+} = \psi_{-}$) can be spontaneously broken if $g > 0$ and E_p exceeds both E_x and E_y [27]. This is a purely dynamical effect, unlike equilibrium phase transitions described by the Landau theory. With increasing field density, the threshold is reached where both $|\psi_{+}|$ and $|\psi_{-}|$ tend to jump sharply, which is attributed to bistability [19]. At the same time, the spin coupling ($\propto g$) makes one of the σ^{\pm} components inhibit or feed the other depending on their phase difference that, in turn, depends on the amplitudes. As a joint effect, it appears that near the threshold an indefinitely small addition to one of $|\psi_{+}|$ or $|\psi_{-}|$ triggers its further growth and the drop of the other component, so that the condensate switches to the state with either right or left circular polarization.

In the previous experiments [22, 27, 37–39], splitting g was comparable to decay rate γ , and the condensate states with broken spin symmetry were stable under constant excitation conditions. Here we assume that g exceeds γ several times (e. g., due to a lateral strain), which alters the system behavior drastically. The spin-asymmetric condensate becomes unstable with respect to the scattering into two modes that are separated from it by finite energy gaps $\pm\Delta E$ and have the same momentum $k = 0$. The two scattered modes are in fact two pairs of coupled same-energy yet opposite-spin Bogolyubov excitations whose coupling and instability are reachable only at sufficiently large g . This differs from the known polariton-polariton scattering processes in which “signal” and “idler” have distinct momenta (e. g., [40–43]). More details and mode diagrams are presented in Appendix B.

Thus, both the spin-symmetric (Π) and asymmetric (Σ_{\pm}) one-mode condensate states can be unstable. The two instabilities meet at, roughly, $g \gtrsim 4\gamma$ and $2\gamma + g/2 \lesssim D \lesssim 2g$, D being the pump detuning from the unsplit polariton level, $D \equiv E_p - E(k=0)$. When these conditions are satisfied, no one-mode states are stable in a finite interval of f , irrespective of the dispersion law and mode structure. This leads, on one hand, to a chaotic behavior of the “dispersionless” polariton condensates in cavity micropillars. On the other hand,

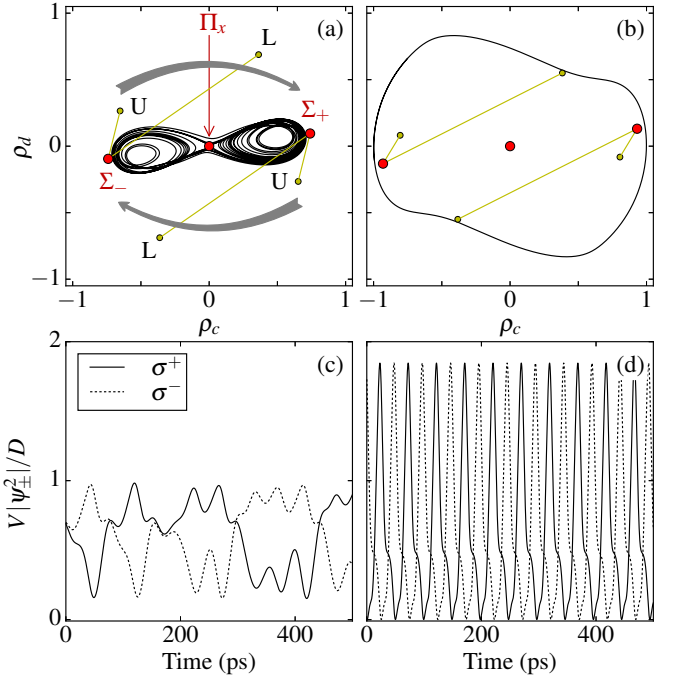


Figure 1. (Color online) Dynamics of a pointlike polariton system. Numerical solutions of Eq. (1) for $2f^2 = 5 \cdot 10^{-4}$ (a, c) and $1.25 \cdot 10^{-3}$ (b, d). (a, b) Phase trajectories over 2000 ps. The large circles indicate the unstable one-mode condensate states (Π_x and Σ_{\pm}). The small circles show the respective lower (L) and upper (U) scattered modes. (c, d) Explicit time dependences of $|\psi_{\pm}|^2$ over 500 ps.

absence of steady plane-wave solutions suggests spontaneous pattern formation in spatially extended systems. These two possibilities are analyzed below.

III. EVOLUTION OF POINTLIKE STATES

Let us consider a pointlike system with $\gamma = 0.02$ meV (like in modern GaAs-based cavities), $g = 10\gamma$, and $D = 7.5\gamma$. Its evolution is described using only three degrees of freedom, $|\psi_{+}|$, $|\psi_{-}|$, and phase difference $\arg \psi_{+}^* \psi_{-}$. The pump is switched on smoothly and then kept constant. All the transient processes vanish in hundreds of picoseconds and are not discussed here. The pump has a small stochastic component whose only purpose is to initiate the symmetry breakdown at the very beginning; it can be arbitrarily small and does not affect the conclusions.

To display phase trajectories [Fig. 1(a), (b)], the Stokes polarization parameters $\rho_c \equiv \rho_{(+,-)}$ and $\rho_d \equiv \rho_{(\cdot,\cdot)}$ are chosen, which are the degrees of circular and $\pm 45^\circ$ linear polarizations; here $\rho_{(a,b)} = (|\psi_a^2| - |\psi_b^2|)/(|\psi_a^2| + |\psi_b^2|)$ by definition. The (x, y) polarization $\rho_l \equiv \rho_{(-,i)}$ can be deduced as the Stokes vector length is unity, $\rho_c^2 + \rho_l^2 + \rho_d^2 = 1$. The positive (negative) sign of ρ_d is indicative of the $\sigma^{-} \rightarrow \sigma^{+}$ ($\sigma^{-} \leftarrow \sigma^{+}$) conversion implied by the linear coupling term in Eq. (1); to make sure, note that $g > 0$ and $\text{sgn}[\text{Im}(\psi_{+}^* \psi_{-})] = \text{sgn}[\rho_d(\psi)]$ for each spinor ψ . In line with this rule, $\text{sgn}(\rho_c) = \text{sgn}(\rho_d)$

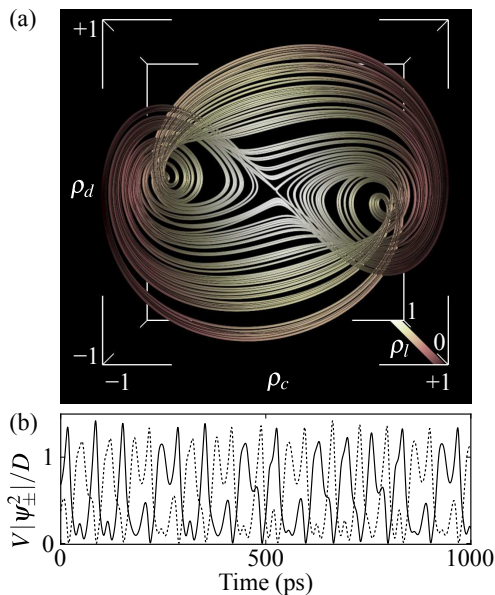


Figure 2. (Color online) Chaotic attractor typical of a pointlike system. (a) Phase trajectory over a 6000 ps interval in the space of the Stokes polarization parameters; the color represents linear polarization ρ_l . (b) Explicit time dependences of $|\psi_{\pm}^2|$ over 1000 ps.

in each of the Σ_{\pm} condensate states. However, the scattered modes appear to have the opposite sign of ρ_d , and thus their filling acts to restore the spin symmetry or even flip the spin, provided they are filled rapidly enough.

The dynamics of a chaotic polariton state [Fig. 1(a), (c)] can be understood as a counteraction between the symmetry breakdown tendency and the instability of the asymmetric states. The two instabilities differ in nature, therefore they cannot balance each other. At lower f (not shown) the system swings between the Π state and one of the Σ_{\pm} states but does not alter the initially “chosen” sign of ρ_c . With increasing f , the growth rate Γ of the scattered modes increases, and so the condensate is able to occasionally flip the spin. Instead of the single—spontaneous and irreversible—symmetry breakdown, one observes an infinite sequence of spin switches; nevertheless, the system is still extremely sensitive to fluctuations near the Π point. Calculations show that an arbitrarily small deflection from any given point of the phase trajectory results in an exponentially divergent trajectory, which is indicative of chaos.

At a stronger pump, Γ becomes so large that it ensures the spin-flip event each time the system reaches a Σ state, and the trajectory takes the form of a limit cycle [Fig. 1(b), (d)]. Maximum Γ is roughly comparable to decay rate γ (e. g., [40, 44]); accordingly, the oscillation period is comparable to the polariton lifetime. With further increasing f (not shown), Γ is reduced, as the coupling of the Bogolyubov excitations decays due to their energy mismatch (this is explained in detail in Appendix B). As a result, chaotic dynamics re-establishes; afterwards it degenerates into one-scroll oscillations and, finally, into a fixed point.

With increasing pump detuning up to $D = g$, the nonlin-

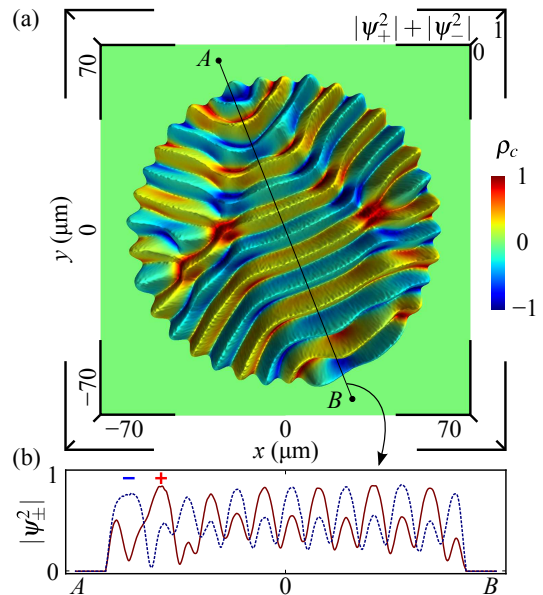


Figure 3. (Color online) Self-organized field in a circular cavity. (a) Full intensity $|\psi_+^2| + |\psi_-^2|$, in arbitrary units, as a function of in-plane coordinates; the color represents circular polarization ρ_c . (b) Explicit spatial dependences of $|\psi_{\pm}^2|$ along the cross section AB .

earity is enhanced and the system behavior becomes chaotic in a wider interval of f . Figure 2 shows the evolution at $D = g = 10\gamma = 0.2$ meV and $2f^2 = 5 \cdot 10^{-4}$. The spin flips are quick and irregular and it is impossible to predict the dominant spin for more or less far future. Even when absolutely no stochastic factors influence the system, prediction of its future states requires an exponentially growing precision. Similar features implemented in lasers were proposed for fast random number generation [2].

IV. SELF-ORGANIZATION AND CHAOS IN PLANAR CAVITIES

Let us now turn to spatially extended polariton systems under one-mode driving. *A priori* it is clear that if such a system keeps being plane-wave, it will fit the already discussed scenario (spatially homogeneous solutions must be rapidly varying), otherwise spatial symmetry will be broken.

To ensure zero boundary conditions, the decay rate γ is set to increase sharply on the edge of a circular area of radius $R = 60 \mu\text{m}$. Hence, the model is $\text{SO}(2)$ -invariant, i. e., rotationally symmetric. Let us note that the anisotropy implied by both the splitting ($g \equiv E_x - E_y$) and x -oriented pump polarization is reflected only in phase difference $\arg \psi_+^* \psi_-$. At the same time, $\psi_+(x, y)$ and $\psi_-(x, y)$ per se are expected to be rotationally symmetric, based on the symmetry of the potential landscape and excitation conditions.

Figure 3 displays the cavity-field distribution obtained at $g = 10\gamma$ and $D = 7.5\gamma$ (as in Fig. 1). In this example, the system comes to a steady but highly nonuniform state in which the continuous $\text{SO}(2)$ symmetry is broken together with the

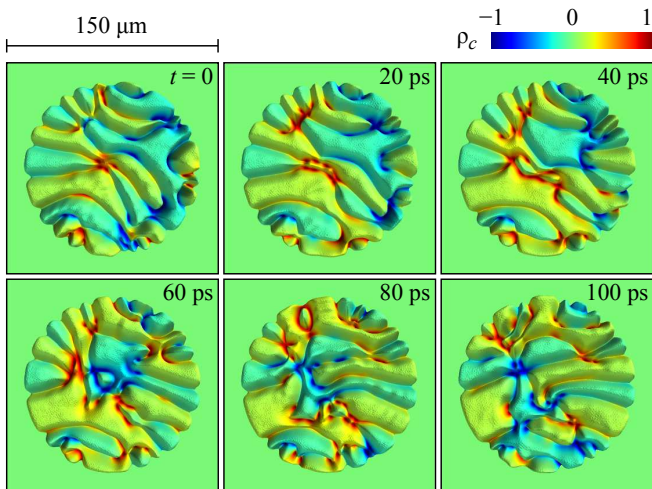


Figure 4. (Color online) Chaotic field evolution. Instantaneous emission snapshots drawn at 20 ps intervals. The color represents circular polarization ρ_c .

spin symmetry. Such solutions are established in hundreds of picoseconds and are spontaneous in that a small fluctuation coming at a critical stage would result in a completely different picture. They are self-organized, i. e., ordered internally, and always “preferred” over rapidly varying homogeneous solutions if it is ever allowed dynamically.

The scale of inhomogeneity is deduced from the wave numbers k_s of the scattered modes. The parametric scattering *from* the condensate always precedes and mediates its switches to high-energy states in bi- or multistable polariton systems [44, 45]. In accordance with the dispersion law and phase-matching conditions, in our system $|k_s|$ may vary from 0 to $\sim 0.4 \mu\text{m}^{-1}$ depending on ψ_{\pm} (see Appendix B). Correspondingly, the cavity field is inhomogeneous on the scale of several microns irrespective of R .

The very intriguing feature of the self-organized cavity field is that it arranges itself into a bunch of wires that have alternating ρ_c and are separated by low-intensity regions. This effect originates in the free flow of polaritons combined with their repulsive interaction, which becomes especially pronounced in spatially distributed bistable systems. For instance, if the switch to the “on” state in such a system proceeds locally, the polariton flow triggers a chain of analogous switches in neighboring places, and eventually the “on” state with a particular spin spreads as far as possible [38, 46]. In our system, the polariton flow acts to expand and, thus, homogenize both the spin-up and spin-down high-density regions. As a result, given that flat and “rapid” two-dimensional patterns are ruled out in favor of self-organized steady states, the only possible outcome of the spin expansion is a set of long-ordered quasi-one-dimensional wires. The *filamentation* is in fact typical of many of spontaneously ordered systems [5, 47].

The spin wires are inevitably destroyed at larger field densities. They always tend to expand in all directions, and so the chaotic dynamics is restored as soon as sufficiently broad homogeneous patterns return in the field distribution. Such

patterns are comparatively narrow in the k space and, hence, internally unstable due to the same reason as the one-mode solutions considered above in Secs. II and III. Figure 4 shows the evolution over a 0.1 ns interval starting at 2.5 ns after the constant pump has been switched on; it is obtained at $g = 15\gamma$ and $D = 12.5\gamma$. The field structure reveals spatiotemporal chaos. It is highly sensitive to fluctuations at all times rather than only at a certain critical stage of pattern formation. At every instant, an arbitrary small and short-range fluctuation would lead to an exponentially divergent evolution branch. As a result, each given location within the cavity plane shows the chaotic behavior.

Thus, beyond a certain critical scale \mathcal{Q} the cavity field cannot be at once steady and spatially homogeneous; furthermore, the inhomogeneous steady states lose stability at higher field densities. An example of a limit-cycle solution with a spontaneous reduction of the $\text{SO}(2)$ symmetry down to C_2 for $R = 10 \mu\text{m}$ is analyzed in Appendix C; it is an intermediate stage between pointlike states and large two-dimensional cavities. With increasing size, closed periodical trajectories cease to exist. It is reasonable that the degree of complexity of such systems infinitely grows with R , in analogy to turbulent fluids [47]. This hypothesis is substantiated, first, by perfectly deterministic character of the model, i. e., the mere fact that complexity does not come from the outer sources of entropy like thermal reservoirs, random potentials, or stochastic forces. On the other hand, enlarging extent does enrich at least a statistical diversity. Numerical estimates show that the first-order spatial correlation function drops rapidly with increasing distance beyond \mathcal{Q} , which suggests statistical independence of remote locations. Nonetheless, the geometry of the high-dimensional chaotic attractors in cavity-polariton systems invites further investigation.

V. CONCLUSION

In summary, we have found the mechanism making spin of light behave as a turbulent fluid. The key point is the spontaneous breakdown of spin symmetry, which brings about an extreme sensitivity to fluctuations in a resonantly excited polariton system. The scattering into Bogolyubov modes acts to close the cycle and triggers an infinite series of spin switches. This mechanism is fundamental; being independent of the potential landscape or the shape of the pump wave, it is expected to take place in arbitrarily sized planar microcavities. As a result, cavities with strong exciton-photon coupling can serve as all-optical free-running chaotic radiation emitters operating on the scale of picoseconds and microns.

ACKNOWLEDGMENTS

I wish to thank N. A. Gippius, S. G. Tikhodeev, and V. D. Kulakovskii for stimulating discussions. The work was supported by the Russian Science Foundation (grant No. 14-12-01372).

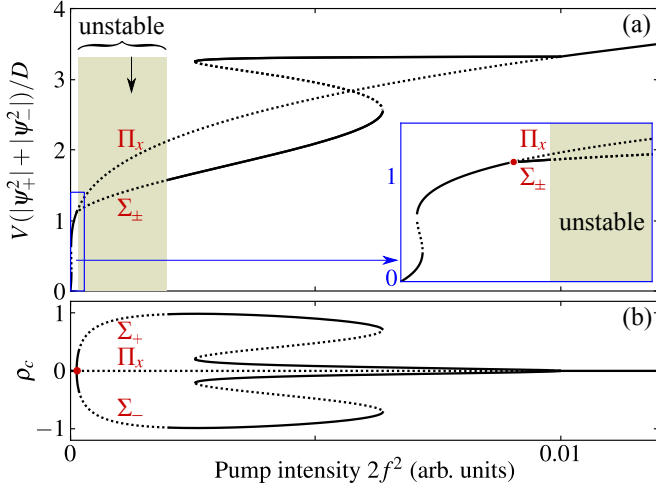


Figure 5. (Color online) (a) One-mode solutions of Eq. (B1), condensate intensity vs. pump intensity. The range of small pump intensities is shown in the inset. Unstable branches are indicated by dotted lines. The interval with no stable solutions is shadowed. (b) Corresponding degrees of circular polarization.

Appendix A: Two-dimensional model

The low-polariton dispersion law reads,

$$E_{\text{LP}}(\mathbf{k}) = \frac{E_C(\mathbf{k}) + E_X}{2} - \frac{1}{2} \sqrt{[E_C(\mathbf{k}) - E_X]^2 + \Re^2}, \quad (\text{A1})$$

where \Re is the exciton-photon coupling rate (Rabi splitting), E_X the exciton energy, and $E_C(\mathbf{k})$ the dispersion law of cavity photons,

$$E_C(\mathbf{k}) = E_C^{(0)} + \frac{\hbar^2 \mathbf{k}^2}{2m_C}, \quad m_C = \frac{\varepsilon E_C^{(0)}}{c^2}. \quad (\text{A2})$$

The exciton effective mass is much larger than m_C , so the k dependence of E_X is neglected. In the real space, energy op-

$$\hat{L} = \begin{pmatrix} E_{\text{LP}}(\mathbf{k}) - i\gamma + 2V|\bar{\psi}_+^2| & V\bar{\psi}_+^2 & g/2 & 0 \\ -V\bar{\psi}_+^{*2} & 2E_p - E_{\text{LP}}(-\mathbf{k}) + i\gamma - 2V|\bar{\psi}_+^2| & 0 & -g/2 \\ g/2 & 0 & E_{\text{LP}}(\mathbf{k}) - i\gamma + 2V|\bar{\psi}_-^2| & V\bar{\psi}_-^2 \\ 0 & -g/2 & -V\bar{\psi}_-^{*2} & 2E_p - E_{\text{LP}}(-\mathbf{k}) + i\gamma - 2V|\bar{\psi}_-^2| \end{pmatrix}. \quad (\text{B4})$$

Below we take $\gamma = 0.02$ meV, $g \equiv E_x - E_y = 10\gamma$, and $D \equiv E_p - E_{\text{LP}}(k=0) = 7.5\gamma$ (as in Figs. 1 and 3). The one-mode solutions $\bar{\psi}_\pm$ are determined using Eq. (B1) in a wide range of f (Fig. 5). Solving the linear problem (B2) for each $\bar{\psi}_\pm$ yields, in each of two spin components, a pair of Bogolyubov excitations obeying phase-matching conditions

$$E_{\text{signal}}(\mathbf{k}) + E_{\text{idler}}(-\mathbf{k}) = 2E_p. \quad (\text{B5})$$

“Signal” and “idler” are widely used designations for such modes in cavity-polariton systems, by analogy with optical

erator \hat{E} takes the form

$$\hat{E} = E_{\text{LP}}(-i\hbar\nabla) + \begin{cases} 0 & \text{at } |\mathbf{r}| \leq R; \\ U & \text{at } |\mathbf{r}| > R. \end{cases} \quad (\text{A3})$$

This is the bare—unperturbed and unsplit—polariton energy substituted into Eq. (1). The jump at $|\mathbf{r}| = R$ enables simulating a finite-sized cavity; it should be just large enough to ensure zero boundary conditions. For instance, qualitatively the same results are obtained for $U = 25$ meV, $U = -25$ meV, and $U = -i \times 25$ meV. The last variant means a jump in the decay rate; it was used in final simulations. The micro-cavity parameters are $E_C^{(0)} = E_X = 1.5$ eV, $\varepsilon = 12.5$, and $\Re = 10$ meV. Eq. (1) was solved on a 250×250 square grid with $-75 < x, y < 75 \mu\text{m}$.

Appendix B: Plane-wave solutions and their asymptotic stability

Since the pump is a plane wave falling perpendicular to the cavity ($k = 0$), the stationary solutions of Eq. (1) are sought for in the form $\psi_\pm(t) = \bar{\psi}_\pm e^{-i(E_p/\hbar)t}$. One obtains the following time-independent equations for $\bar{\psi}_+$ and $\bar{\psi}_-$:

$$[E_p - (E_{\text{LP}}(k=0) - i\gamma) - V\bar{\psi}_\pm^* \bar{\psi}_\pm] \bar{\psi}_\pm - \frac{g}{2} \bar{\psi}_\mp - f = 0. \quad (\text{B1})$$

Stability analysis is performed by linearizing Eq. (1) over small deflections from the one-mode solutions. In the k space this leads to the 4×4 linear problem

$$\hat{L}\Psi = E\Psi, \quad \text{where} \quad (\text{B2})$$

$$\Psi = [\psi_+(\mathbf{k}), \psi_+^*(-\mathbf{k}), \psi_-(\mathbf{k}), \psi_-^*(-\mathbf{k})]^T, \quad (\text{B3})$$

parametric oscillators. Eq. (B5) means energy and momentum conservation in the course of the two-particle scattering from the pumped mode, $(p, p) \rightarrow (s, i)$. The real and imaginary parts of the eigenvalues of matrix (B4) determine, respectively, the energy levels and decay rates of the excitations; a positive imaginary part means instability. The Stokes polarization parameters are determined by the respective eigenvectors. Figure 5 intentionally does not take account of the scattering into $k \neq 0$; in other words, it shows only the one-mode (in)stability.

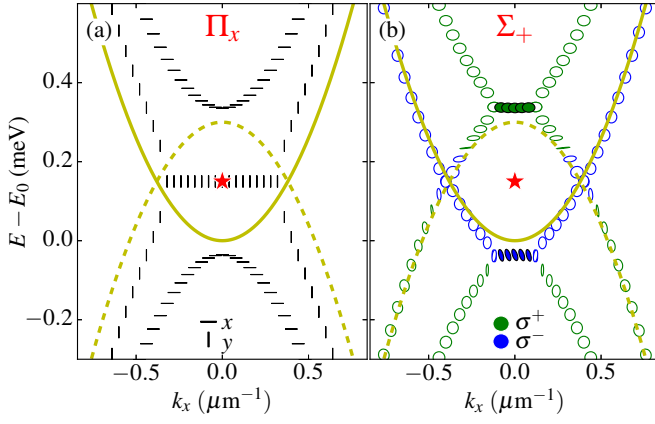


Figure 6. (Color online) Bogolyubov excitations in the Π_x (a) and Σ_+ (b) one-mode states at $2f^2 = 1.25 \cdot 10^{-3}$ [the pump intensity is marked by the vertical arrow at the top of Fig. 5(a)]. Stars indicate the condensate mode at $k = 0$, $E = E_p$. Lines show the reference (unsplit) dispersion law $E_{LP}(k)$ (solid line) and its “idler” counterpart $2E_p - E_{LP}(-k)$ (dashed line). Strips and ellipses represent polarization states. Full ellipses in (b) indicate unstable modes.

The range of low pump amplitudes is shown in the inset of Fig. 5(a). The pump polarization (x) matches exactly the upper eigenstate at $\psi_{\pm} \rightarrow 0$ which is, hence, the only occupied state at small f . At the very beginning the response is linear and afterwards it takes the form of an S-shaped curve. Since $E_p - E_x$ exceeds $\sqrt{3}\gamma$, the system is *bistable* [11, 20, 44], which stems from the positive feedback loop between the amplitude ($|\psi_x|$) and effective resonance frequency ($E_x + V|\psi_x|^2$) in a finite range of $|\psi_x|$.

With increasing f , the nonlinear terms in Eq. (1) couple the x and y polarization components. As a result, one-mode solutions with a nonzero fraction of the “unpumped” (y) component become possible along with purely x -polarized states. That is why the upper stability branch splits into three, of which one (Π_x) remains polarized linearly in the x direction and the other two (Σ_{\pm}) acquire large and mutually opposite circular polarizations. All these one-mode branches are unstable over a wide interval of f . The excitations in the Π_x and Σ_+ states near the center of that interval are outlined in Fig. 6.

Branch Π and the symmetry breakdown.—Figure 6(a) reveals the y -polarized “signal” and “idler” stuck together within a wide flat area centered at $E = E_p$. Since the real parts of their energies coincide, the imaginary parts diverge and one of them takes a positive value; this is quite a general property of Eq. (1) [40]. Thus, on branch Π_x the condensate is unstable *in itself*: its y -polarization component tends to jump sharply. Consequently, the field has to acquire an elliptical polarization, but Fig. 6(a) suggests nothing about its *sense*; the spin-up (Σ_+) and spin-down (Σ_-) condensate states that could arise as a result of such instability are in fact equally probable [27].

Branch Σ and coupled Bogolyubov modes.—The Σ states of the condensate are stable at comparatively small g . The excitations at $k = 0$ were previously known to be occupied in the course of transient processes but not in a steady state, as they

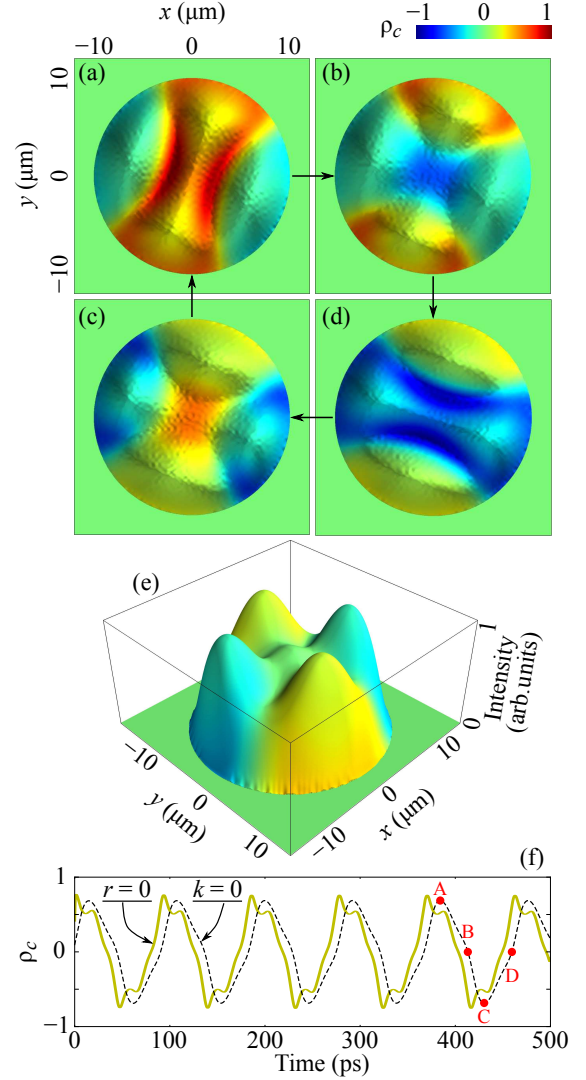


Figure 7. (Color online) Periodic solution for $R = 10 \mu\text{m}$. (a)–(d) Instantaneous spin and intensity patterns; (e) the pattern averaged over the period. (f) Time dependences of ρ_c in the $\mathbf{r} = 0$ point of the real space (solid line) and $\mathbf{k} = 0$ point of the momentum space (dashed line). The time moments represented in panels (a)–(d) are marked as A–D.

were decaying [48]. Increasing g brings about unstable (non-decaying) modes below and above the condensate as seen in Fig. 6(b).

The bottom row of unstable modes is found near the weakly populated and, thus, unshifted level of the minor spin component (σ^- in our example). Approximately the same energy corresponds to a significantly red-shifted σ^+ -polarized “idler”, if we accept that conventional idlers form the downward branches. The opposite-spin signals and idlers with nearly coincident energies stick together and so they make up the flattened k -space region and acquire positive growth rates $\Gamma \equiv \text{Im } E$. As said above, it is possible only at comparatively large opposite-spin coupling g .

The greater the amplitude, the stronger the blue (red) shift of the signal (idler). With increasing f , the major-spin idler

goes far below $E_0 = E_{LP}(k=0)$ and is no longer able to hybridize with the other—always weak and unshifted—spin component because of their energy mismatch. As a result, the one-mode Σ_{\pm} states cannot break up anymore and, thus, restore their stability. In general, there is the other way to restore stability at larger f [Fig. 5] via a jump in *both* σ^{\pm} components in spite of the symmetry breaking forces; this, however, does not happen in the considered parameter range.

Appendix C: Periodic states in small cavities

Let us consider an intermediate case between pointlike states and large planar systems. The solution sketched out in Fig. 7 is obtained for a small circular cavity with $R = 10 \mu\text{m}$. The parameters are $D = g = 10\gamma = 0.2 \text{ meV}$ and $2f^2(k=0) = 3 \cdot 10^{-3}$. They lead to the area with no steady-state solutions; in the outer areas the spin and intensity distributions are always constant in time and rotationally invariant.

Figure 7 shows that (i) the SO(2) symmetry is spontaneously reduced down to C_2 , (ii) the spin symmetry is broken,

and (iii) the space pattern oscillates with a period of $T \approx 90 \text{ ps}$. The distinctive stages of the cycle are shown in Figs. 7(a)–(d). The field is anisotropic even after averaging over the period [Fig. 7(e)]. It exhibits a pair of orthogonal directions that are spontaneously chosen at the moment of symmetry breaking.

Figure 7(f) shows the dynamics of the circular-polarization degree in the $\mathbf{r} = 0$ point of the real space and in the $\mathbf{k} = 0$ point of the momentum space. Both have the amplitude of about 0.7. The integral polarization,

$$\bar{\rho}_c = \frac{I_+ - I_-}{I_+ + I_-}, \quad \text{where} \quad I_{\pm}(t) = \int |\psi_{\pm}(\mathbf{r}, t)|^2 d\mathbf{r},$$

has a smaller oscillation amplitude of 0.25 (not shown); the full intensity $I_+(t) + I_-(t)$ also varies with time within about 10%. Thus, the evolution is reduced to neither plain temporal oscillations typical of micropillars nor a periodic spatial redistribution with invariant integral characteristics that would be rather typical of the Josephson effect in Hermitian systems.

The island-like patterns grow into the spin wires with increasing R . On the other hand, increasing density at greater g and $D \sim g$ would homogenize the system, thereby making it similar to plain pointlike states in small cavity micropillars.

-
- [1] M. Virte, K. Panajotov, H. Thienpont, and M. Sciamanna, *Nat Photon* **7**, 60 (2013).
 - [2] M. Sciamanna and K. A. Shore, *Nat Photon* **9**, 151 (2015).
 - [3] D. Colas, L. Dominici, S. Donati, A. A. Pervishko, T. C. H. Liew, I. A. Shelykh, D. Ballarini, M. de Giorgi, A. Bramati, G. Gigli, E. del Valle, F. P. Laussy, A. V. Kavokin, and D. Sanvitto, *Light Sci Appl* **4**, e350 (2015).
 - [4] G. Tosi, G. Christmann, N. Berloff, P. Tsotsis, T. Gao, Z. Hatzopoulos, P. Savvidis, and J. Baumberg, *Nat Commun* **3**, 1243 (2012).
 - [5] M. C. Cross and P. C. Hohenberg, *Rev. Mod. Phys.* **65**, 851 (1993).
 - [6] C. Weisbuch, M. Nishioka, A. Ishikawa, and Y. Arakawa, *Phys. Rev. Lett.* **69**, 3314 (1992).
 - [7] Y. Yamamoto, T. Tassone, and H. Cao, *Semiconductor Cavity Quantum Electrodynamics* (Springer-Verlag, 2000).
 - [8] A. V. Kavokin, J. J. Baumberg, G. Malpuech, and P. Laussy, *Microcavities* (Oxford University Press, 2007).
 - [9] J. Kasprzak, M. Richard, S. Kundermann, A. Baas, P. Jembarun, J. M. J. Keeling, F. M. Marchetti, M. H. Szymanska, R. André, J. L. Staehli, V. Savona, P. B. Littlewood, B. Deveaud, and L. S. Dang, *Nature* **443**, 409 (2006).
 - [10] R. Balili, V. Hartwell, D. Snoke, L. Pfeiffer, and K. West, *Science* **316**, 1007 (2007).
 - [11] V. F. Elesin and Y. V. Kopayev, *Sov. Phys. JETP* **36**, 767 (1973).
 - [12] H. Haug and H. H. Kranz, *Zeitschrift für Physik B Condensed Matter* **53**, 151 (1983).
 - [13] B. Josephson, *Physics Letters* **1**, 251 (1962).
 - [14] S. Levy, E. Lahoud, I. Shomroni, and J. Steinhauer, *Nature* **449**, 579 (2007).
 - [15] K. G. Lagoudakis, B. Pietka, M. Wouters, R. André, and B. Deveaud-Plédran, *Phys. Rev. Lett.* **105**, 120403 (2010).
 - [16] M. Abbarchi, A. Amo, V. G. Sala, D. D. Solnyshkov, H. Flayac, L. Ferrier, I. Sagnes, E. Galopin, A. Lemaître, G. Malpuech, and J. Bloch, *Nat Phys* **9**, 275 (2013).
 - [17] I. A. Shelykh, D. D. Solnyshkov, G. Pavlovic, and G. Malpuech, *Phys. Rev. B* **78**, 041302 (2008).
 - [18] N. A. Gippius, I. A. Shelykh, D. D. Solnyshkov, S. S. Gavrilov, Y. G. Rubo, A. V. Kavokin, S. G. Tikhodeev, and G. Malpuech, *Phys. Rev. Lett.* **98**, 236401 (2007).
 - [19] S. S. Gavrilov, N. A. Gippius, S. G. Tikhodeev, and V. D. Kulakovskii, *JETP* **110**, 825 (2010).
 - [20] A. Baas, J. P. Karr, H. Eleuch, and E. Giacobino, *Phys. Rev. A* **69**, 023809 (2004).
 - [21] N. A. Gippius, S. G. Tikhodeev, V. D. Kulakovskii, D. N. Krizhanovskii, and A. I. Tartakovskii, *EPL* **67**, 997 (2004).
 - [22] T. K. Paraiso, M. Wouters, Y. Léger, F. Morier-Genoud, and B. Deveaud-Plédran, *Nat Mater* **9**, 655 (2010).
 - [23] D. Sarkar, S. S. Gavrilov, M. Sich, J. H. Quilter, R. A. Bradley, N. A. Gippius, K. Guda, V. D. Kulakovskii, M. S. Skolnick, and D. N. Krizhanovskii, *Phys. Rev. Lett.* **105**, 216402 (2010).
 - [24] C. Adrados, A. Amo, T. C. H. Liew, R. Hivet, R. Houdré, E. Giacobino, A. V. Kavokin, and A. Bramati, *Phys. Rev. Lett.* **105**, 216403 (2010).
 - [25] S. Gavrilov, A. Brichkin, A. Dorodnyi, S. Tikhodeev, N. Gippius, and V. Kulakovskii, *JETP Letters* **92**, 171 (2010).
 - [26] S. S. Gavrilov, A. S. Brichkin, A. A. Demenev, A. A. Dorodnyy, S. I. Novikov, V. D. Kulakovskii, S. G. Tikhodeev, and N. A. Gippius, *Phys. Rev. B* **85**, 075319 (2012).
 - [27] S. S. Gavrilov, A. V. Sekretenko, S. I. Novikov, C. Schneider, S. Höfling, M. Kamp, A. Forchel, and V. D. Kulakovskii, *APL* **102**, 011104 (2013).
 - [28] H. Ohadi, A. Dreismann, Y. G. Rubo, F. Pinsker, Y. del Valle-Inclan Redondo, S. I. Tsintzos, Z. Hatzopoulos, P. G. Savvidis, and J. J. Baumberg, *Phys. Rev. X* **5**, 031002 (2015).
 - [29] D. Sarchi, I. Carusotto, M. Wouters, and V. Savona, *Phys. Rev. B* **77**, 125324 (2008).
 - [30] D. D. Solnyshkov, R. Johne, I. A. Shelykh, and G. Malpuech, *Phys. Rev. B* **80**, 235303 (2009).
 - [31] E. B. Magnusson, H. Flayac, G. Malpuech, and I. A. Shelykh,

- Phys. Rev. B **82**, 195312 (2010).
- [32] I. Iorsh, A. Alodjants, and I. A. Shelykh, *Opt. Express* **24**, 11505 (2016).
- [33] C. Ciuti, V. Savona, C. Piermarocchi, A. Quattropani, and P. Schwendimann, *Phys. Rev. B* **58**, 7926 (1998).
- [34] P. Renucci, T. Amand, X. Marie, P. Senellart, J. Bloch, B. Sermage, and K. V. Kavokin, *Phys. Rev. B* **72**, 075317 (2005).
- [35] M. Vladimirova, S. Cronenberger, D. Scalbert, K. V. Kavokin, A. Miard, A. Lemaître, J. Bloch, D. Solnyshkov, G. Malpuech, and A. V. Kavokin, *Phys. Rev. B* **82**, 075301 (2010).
- [36] A. V. Sekretenko, S. S. Gavrilov, and V. D. Kulakovskii, *Phys. Rev. B* **88**, 195302 (2013).
- [37] S. S. Gavrilov, A. V. Sekretenko, N. A. Gippius, C. Schneider, S. Höfling, M. Kamp, A. Forchel, and V. D. Kulakovskii, *Phys. Rev. B* **87**, 201303 (2013).
- [38] A. V. Sekretenko, S. S. Gavrilov, S. I. Novikov, V. D. Kulakovskii, S. Höfling, C. Schneider, M. Kamp, and A. Forchel, *Phys. Rev. B* **88**, 205302 (2013).
- [39] S. S. Gavrilov, A. S. Brichkin, S. I. Novikov, S. Höfling, C. Schneider, M. Kamp, A. Forchel, and V. D. Kulakovskii, *Phys. Rev. B* **90**, 235309 (2014).
- [40] C. Ciuti, P. Schwendimann, and A. Quattropani, *Semiconductor Science and Technology* **18**, S279 (2003).
- [41] I. Carusotto and C. Ciuti, *Phys. Rev. Lett.* **93**, 166401 (2004).
- [42] D. M. Whittaker, *Phys. Rev. B* **71**, 115301 (2005).
- [43] D. D. Solnyshkov, I. A. Shelykh, N. A. Gippius, A. V. Kavokin, and G. Malpuech, *Phys. Rev. B* **77**, 045314 (2008).
- [44] S. S. Gavrilov, *Phys. Rev. B* **90**, 205303 (2014).
- [45] S. S. Gavrilov, A. S. Brichkin, Y. V. Grishina, C. Schneider, S. Höfling, and V. D. Kulakovskii, *Phys. Rev. B* **92**, 205312 (2015).
- [46] T. C. H. Liew, A. V. Kavokin, and I. A. Shelykh, *Phys. Rev. Lett.* **101**, 016402 (2008).
- [47] T. Bohr, M. H. Jensen, G. Paladin, and A. Vulpiani, *Dynamical Systems Approach to Turbulence* (Cambridge University Press, 1998).
- [48] A. S. Brichkin, S. G. Tikhodeev, S. S. Gavrilov, N. A. Gippius, S. I. Novikov, A. V. Larionov, C. Schneider, M. Kamp, S. Höfling, and V. D. Kulakovskii, *Phys. Rev. B* **92**, 125155 (2015).